JOURNAL OF Materials CHEMISTRY

Complex formation of ethylenedioxyethylenedithiotetrathiafulvalene (EDOEDT-TTF: EOET) and its self-assembling ability

Gunzi Saito,*[a] Hiroshi Sasaki,[a] Takashi Aoki,[a] Yukihiro Yoshida,*[a] Akihiro Otsuka,[a] Hideki Yamochi,[a,b] Olga O. Drozdova,[a]†‡ Kyuya Yakushi,[c] Hiroshi Kitagawa[d]§ and Tadaoki Mitani[d]

[a]*Division of Chemistry, Graduate School of Science, Kyoto University, Sakyo-ku, Kyoto 606-8502, Japan. E-mail: saito@kuchem.kyoto-u.ac.jp; yoshiday@kuchem.kyoto-u.ac.jp*
[b]*CREST, Japan Science and Technology Corporation (JST), Japan*
[c]*Institute for Molecular Science, Myodaiji, Okazaki 444-8585, Japan*
[d]*Japan Advanced Institute of Science and Technology, Tatsunokuchi, Ishikawa 923-1292, Japan*

Received 19th November 2001, Accepted 14th March 2002
First published as an Advance Article on the web 18th April 2002

36 kinds of donor(D)–acceptor(A) type charge transfer (CT) solids were prepared based on ethylenedioxyethylenedithiotetrathiafulvalene (EDOEDT-TTF or EOET), which is a hybrid molecule of bis(ethylenedioxy)-TTF (BEDO-TTF or BO) and bis(ethylenedithio)-TTF (BEDT-TTF or ET). A plot of the first CT absorption bands in solids against the difference in first redox potential between donor and acceptor molecules (ΔE) classified the complexes into five groups, **A**: highly conductive CT complexes with partial CT state and segregated stacks, **B**: partially ionic CT insulators with alternating stacks, **C**: essentially neutral clathrate complexes, **D**: neutral CT insulators with alternating stacks, and **E**: completely ionic insulators. Group **A** is spread out over an extensive ΔE range compared to one-dimensional organic metals such as the 1 : 1 TTF–TCNQ system. This indicates that the EOET complexes among this group have a high electronic dimensionality arising from the self-aggregation of the EOET molecules in a fashion similar to the BO ones. However, the self-assembling ability of the EOET molecules is less pronounced than that of the BO ones, thereby giving a metal–insulator transition for many complexes among Group **A**. The reduced self-assembling ability also affords alternating stacks in $(MeO)_2TCNQ$, BTDA-TCNQ (Group **B**) and *p*-iodanil (Group **C**) complexes. Two structurally distinct complexes were prepared with spherical C_{60} (Group **D**), one containing concave EOET molecules and one-dimensional C_{60} columns, and the other planar EOET and two-dimensional C_{60} layers. The F_4TCNQ complex (Group **E**) exhibits an antiferromagnetic ordering below 7 K, which is intermediate between those in (BO)(F_4TCNQ) (5.4 K) and (ET)(F_4TCNQ) (14 K).

1 Introduction

Conducting charge transfer (CT) compounds based on bis(ethylenedithio)tetrathiafulvalene (BEDT-TTF or ET) or bis(ethylenedioxy)-TTF (BEDO-TTF or BO) (the main compounds in this paper are presented in Chart 1) have so far offered a number of fascinating materials and phenomena that give rise to new concepts in the field of materials science.[1] For example, (1) *d*-wave type superconductivity claimed for some ET superconductors,[2] (2) a new technique applied on many two-dimensional ET metals to investigate the Fermi-surface topology (*i.e.*, angular dependent magnetoresistance oscillation),[3] (3) a metallic mono- or multilayer fabricated at the air–water interface using BO compounds,[4] (4) metallic and transparent polycarbonate composite films prepared by halogen doped BO.[5]

These fascinating materials and phenomena are largely attributed to the intermolecular interactions between the particular donor molecules (ET or BO), which essentially depend on the characteristics of the component molecules. Hereinafter, intermolecular interactions in connection with the crystal and electronic structures of ET and BO will be separately reviewed.

ET molecules have afforded more than 50 superconductors and a wide variety of one- to two-dimensional metallic and semiconducting compounds.[6] In the solids the ET molecules pile up with sliding overlap in order to minimize the steric hindrance by the terminal ethylene groups which have great conformational freedom. This results in weakened face-to-face π-intermolecular interactions. On the other hand, the molecule has a strong tendency to form a variety of intermolecular sulfur-to-sulfur (S···S) atomic contacts along the side-by-side direction. Thus the two-dimensional crystal and electronic structures are established as a compromise of these two kinds of medium intermolecular interactions. Moreover, there are a variety of donor–anion and anion–anion intermolecular interactions in the ET compounds in addition to the donor–donor ones, thereby giving numerous molecular packing patterns of the ET molecules and hence the presence of polymorphism, complex isomerism, clathrate character or various molecular compositions in the compounds.

The BO molecules have afforded a number of two-dimensional metals including two superconductors.[7] Many BO compounds exhibit metallic behavior down to low temperatures even in severely disordered systems such as compressed pellets, Langmuir–Blodgett (LB) films and composite

†On leave from A. F. Ioffe Physico-Technical Institute, Russian Academy of Science, 194021 St. Petersburg, Russia.
‡*Present address*: Department of Physics, University of Florida, USA.
§*Present address*: Department of Chemistry, University of Tsukuba, Japan.

 DOI: 10.1039/b110605h

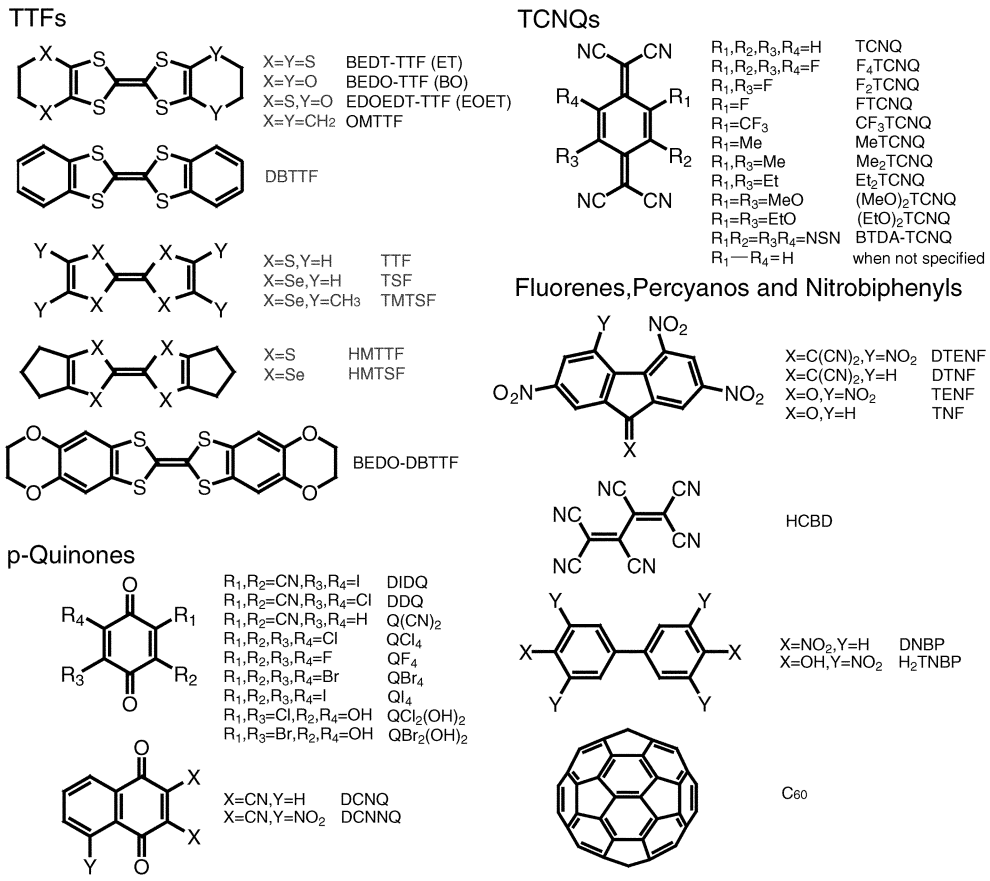

Chart 1 Chemical structures of donor and acceptor molecules in the text.

polymer films,[4,5,7] while the ET compounds in such sample forms are prevented from showing metallic behavior at low temperatures. The exceptional stability of the metallic state in the BO compounds is attributed to the strong donor–donor interactions (self-assembling ability) of BO molecules, which are established by the combination of the short intermolecular CH···O atomic contacts along the stacking direction and the robust $S_{in}\cdots S_{in}$ (S_{in}: sulfur atom in the TTF skeleton) atomic contacts along the side-by-side direction. As a result, the BO molecules crystallize with a limited number of packing patterns giving the structurally and electronically two-dimensional structures. Owing to the negligible or otherwise rather small transfer interactions along the stacking axis, the two-dimensional nature is accomplished by the multiple transfer interactions oblique to the stacking axis. The bandwidth of the HOMO band (0.9–1.2 eV)[7a] is slightly more than that of θ-type ET compounds (0.8–0.9 eV)[8] and the notable stability of the metallic state prevents the occurrence of the superconducting state.

Thus it is of interest to investigate the characteristics of the hybrid molecule of BO and ET—*i.e.* ethylenedioxyethylenedithio-TTF (EDOEDT-TTF or EOET). This molecule is anticipated to exhibit a reduced self-assembling ability in the compounds and a decreased bandwidth compared to those in the BO compounds. Moreover, the decrease in molecular symmetry would facilitate the localization of itinerant electrons due to the existence of disorder and/or non-periodicity in solids. Keeping in mind these expected features, we report here mainly the structural properties of the EOET complexes with organic acceptor molecules to demonstrate the structural diversity. A preliminary study has been previously reported.[9]

EOET was first synthesized by Kini *et al.* in 1990.[10] They argued that the electrochemical property of the EOET molecule is influenced by both parent molecules BO and ET, *i.e.*, the first redox potential ($E^1_{1/2}$(D)) of the molecule is midway between those of the parent molecules. However, experimental work on EOET complexes remains sparse because of the difficulty in attaining the solids. At present, only the following reports have appeared, (1) structural works on EOET itself,[10] C_{60} complex,[11] and AuI_2 (τ- and β-phases)[12] and Hg_3Br_8[13] salts, (2) conducting works on a complex with behenic acid,[14] and AuI_2 (τ- and β-phases),[12] $Cu(NCS)_2$,[12,15] $Pt(CN)_4$,[16] and $Pd(CN)_4$[16] salts, as well as (3) preparation of I_3 and IBr_2 salts,[17] and 7,7,8,8-tetracyano-*p*-quinodimethane (TCNQ) complex.[17,18]

2 Results and discussion

2.1 Electron-donating strength

The electron-donating strength of the EOET molecule is evaluated on the basis of the $E^1_{1/2}$(D) value and the CT transition energy of the *sym*-trinitrobenzene (TNB) complex in solution ($h\nu_{CT}^{soln}$). Both the $E^1_{1/2}$(D) (+0.47 V *vs.* saturated calomel electrode (SCE)) and the $h\nu_{CT}^{soln}$ values (15.5×10^3 cm^{-1} in $CHCl_3$) are midway between those of parents, BO ($E^1_{1/2}$(D) = +0.43 V, $h\nu_{CT}^{soln} = 15.0 \times 10^3$ cm^{-1}) and ET ($E^1_{1/2}$(D) = +0.53 V, $h\nu_{CT}^{soln} = 16.1 \times 10^3$ cm^{-1}), indicating that the electron-donating ability of EOET is also midway between those of BO and ET as reported previously.[10,18] The difference between the second and first redox potentials (0.26 V) is closely similar to those of BO (0.26 V) and ET (0.25 V), implying a comparable bare on-site Coulomb repulsive energy (U_0) between them.

2.2 Classification of charge transfer complex

Table 1 summarizes the results of the complex formation: acceptor molecules with their first redox potential ($E^1_{1/2}$(A) *vs.* SCE), the difference in first redox potentials between EOET and each acceptor molecule ($\Delta E = E^1_{1/2}(D) - E^1_{1/2}(A)$),

Table 1 Appearance, stoichiometry, optical and conductivity data of EOET complexes together with redox potentials ($E^1_{1/2}$(A) and ΔE = $E^1_{1/2}$(EOET) − $E^1_{1/2}$(A))

No.	Acceptor[a]	$E^1_{1/2}$(A)[b]/V	ΔE[c]/V	Appearance[d]	D : A : (solv)[e]	$h\nu_{CT}{}^{solid}$[f]/10^3 cm^{-1}	σ_{RT}/S cm^{-1} [ε_a/meV], T_{MI}[g]
1a	HCBD	0.72	–0.25	Dark green pwd	—	3.4	12(P), T_{MI} = 120 K
1b	HCBD	0.72	–0.25	Black blue pwd	1 : 1	11.3	$<10^{-8}$
2	F_4TCNQ	0.60	–0.13	Black needle	1 : 1	6.7	1.8×10^{-6}(P) [160]
3	DDQ	0.56	–0.10	Brown pwd	7 : 8 : 2(H_2O)	3.4	6.7×10^{-1}(P) [16]
4	DIDQ	0.51	–0.04	Brown pwd	2 : 1 : 0.5(H_2O)	3.6	3.6(P) [25]
5	CF_3TCNQ	0.44	0.03	Green pwd	2 : 1	3.2	5.8(P), T_{MI} = 250 K
6	F_2TCNQ	0.41	0.06	Green polycry	2 : 1 : 1(H_2O)	3.5	35(P), T_{MI} = 15 K
7	DCNNQ	0.38	0.09	Black pwd	7 : 4 : 4(H_2O)	4.0	2.3×10^{-1}(P) [76]
8	$Q(CN)_2$	0.35	0.11	Brown pwd	—	5.9	$<10^{-8}$
9	FTCNQ	0.32	0.15	Black polycry	1 : 1	3.4	7.7(P), T_{MI} = 100 K
10	DTENF	0.23	0.24	Dark green pwd	2 : 1 : 1(AN)	3.2	8.3×10^{-1}(P) [120]
11	TCNQ	0.22	0.25	Black plate	1 : 1	3.3	7.7, T_{MI} = 165–100 K
12	DCNQ	0.21	0.26	Brown pwd	2 : 1	3.8	3.5(P) [30]
13	MeTCNQ	0.19	0.28	Black polycry	4 : 3	3.3	1.3(P) T_{MI} = 100 K
14	Et_2TCNQ	0.15	0.32	Green pwd	2 : 1	2.9	15(P) T_{MI} = 120 K
15	Me_2TCNQ	0.15	0.32	Black pwd	1 : 1	6.0	$<10^{-8}$
16	$(MeO)_2$TCNQ	0.05	0.42	Black plate	2 : 1	6.4	$<10^{-8}$
17	QCl_4	0.05	0.42	Brown pwd	8 : 9 : 1(H_2O)	4.0	2.9(P), T_{MI} = 200 K
18a	QF_4	0.04	0.43	Dark brown pwd	—	4.8	3.1×10^{-3}(P) [130]
18b	QF_4	0.04	0.43	Black pwd	—	11.8	$<10^{-8}$
19	QBr_4	0.04	0.43	Black polycry	3 : 2	11.1	$<10^{-8}$
20a	BTDA-TCNQ	0.03	0.44	Black pwd	3 : 2	2.1	23(P), T_{MI} = 200 K
20b	BTDA-TCNQ	0.03	0.44	Black needle	1 : 1	7.6	$<10^{-8}$
20c	BTDA-TCNQ	0.03	0.44	Black plate	1 : 2	7.0	$<10^{-8}$
21	DTNF	0.02	0.45	Green pwd	1 : 1	8.2	3.2×10^{-9} [420]
22	$(EtO)_2$TCNQ	0.01	0.46	Dark brown pwd	2 : 1	8.1	$<10^{-8}$
23	QI_4	−0.02	0.49	Black plate	2 : 1	9.9	$<10^{-8}$
24a	$QBr_2(OH)_2$	−0.12	0.59	Black polycry	—	3.4	14, T_{MI} = 260 K
24b	$QBr_2(OH)_2$	−0.12	0.59	Black pwd	—	10.7	$<10^{-8}$
25	$QCl_2(OH)_2$	−0.13	0.60	Light brown pwd	—	3.3	1.8(P) [24]
26	TENF	−0.14	0.61	Black pwd	—	11.1	$<10^{-8}$
27	TNF	−0.43	0.89	Black block	4 : 3	10.7	$<10^{-8}$
28a	C_{60}	−0.44	0.90	Black block	1 : 1 : 1(Bz)	11.8	$<10^{-8}$
28b	C_{60}	−0.44	0.90	Black plate	1 : 1 : 1(Bz)	11.8	$<10^{-8}$
29	H_2TNBP	−0.56	1.03	Black polycry	—	12.0	$<10^{-8}$
30	DNBP	−0.98	1.45	Black plate	6 : 5	14.8	$<10^{-8}$

[a]See Chart 1. [b]First redox potential of acceptor *vs.* SCE. [c]Difference in first redox potential between donor and acceptor. [d]pwd: powder, polycry: polycrystals. [e]By elemental or structural analysis, AN: acetonitrile, Bz: benzene, —: not known. [f]First CT absorption band in KBr pellet. [g]T_{MI}: metal–insulator transition temperature, P: pellet sample.

appearance, stoichiometry, the first CT absorption band in KBr pellet ($h\nu_{CT}{}^{solid}$), and the conductivity at RT (σ_{RT}) together with the activation energy (ε_a) or temperature at which metal–insulator (MI) transition occurs (T_{MI}).

Fig. 1 plots the $h\nu_{CT}{}^{solid}$ values against the ΔE ones for the EOET complexes obtained. The numbering for the complexes follows the order of electron-accepting ability of the acceptor molecules. The right- and left-hand sides of the V-shaped line represent the theoretical CT transition energies for neutral ($h\nu_{CT}{}^{N}$) and ionic ($h\nu_{CT}{}^{I}$) CT solids with D–A alternating stacks, respectively,[19] whereas the low-lying bands below 5×10^3 cm^{-1} (horizontal dashed line) are generally attributed to an intermolecular transition between the same component species with partially ionic ground state,[7a,20,21] which is required for the conducting materials. Based on these assignments, the EOET complexes could be classified into the following five categories (Groups **A**–**E**). Interestingly, some particular combinations of component molecules provide multiple phases concerning the stoichiometry, structure, and/or conductivity (**1a–1b**, **18a–18b**, **20a–20c**, **24a–24b**, **28a–28b**), and these complexes except **1** and **28** locate in the vicinity of the right vertical line (*vide infra*) as shown in Fig. 1. Such phenomena, *i.e.* polymorphism, complex isomerization, monotropic neutral–ionic isomers, and so forth,[22,23] have also been reported for the BEDO-DBTTF,[20] ET,[24] TSF[25] and TMTSF[26] systems but rarely for the BO system.

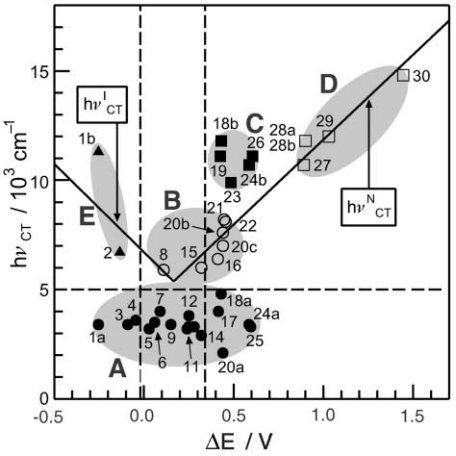

Fig. 1 A plot of the first transition energy in solid ($h\nu_{CT}{}^{solid}$) against the difference in redox potential between EOET and acceptor molecules (ΔE). For the V-shaped line, and the vertical and horizontal dotted lines, see text. Numbers correspond to those in the first column of Table 1. ●: Group **A**, ○: Group **B**, ■: Group **C**, □: Group **D**, ▲: Group **E**.

Group A. 17 highly conductive complexes (**1a**, **3–7**, **9–14**, **17**, **18a**, **20a**, **24a**, **25**) with the low-lying CT band below 5×10^3 cm^{-1}, are obtained in the following redox region:

$$-0.25 \leqslant \Delta E \leqslant 0.60 \text{ V} \quad (1)$$

This range is much wider compared to that of the 1 : 1 TTF–TCNQ system, as represented by the two vertical dotted lines in Fig. 1 or eqn. (2).[23]

$$-0.02 \leqslant \Delta E \leqslant 0.34 \text{ V} \quad (2)$$

The extension of the lower limit in ΔE is apparently owing to the formation of non 1 : 1 stoichiometry (**3**, **4**), in which the excess component would be in a partially ionized state. On the other hand, the extension of the upper limit is indicative of a higher electronic dimensionality than that of the TTF–TCNQ system, as demonstrated in the BO compounds.[7a,27] As far as the plot of $h\nu_{CT}^{solid}$ against ΔE is concerned, the highly conductive region in the EOET system is almost identical to that in the BO system,[7a] indicating the existence of the strong self-assembling ability of the EOET molecules.

Indeed, the temperature dependence of resistivity of the complexes in this group is metallic, although they exhibit a MI transition. The presence of the MI transition in many EOET complexes indicates a weaker self-assembling ability compared to that of the BO compounds in which such a transition has been rarely found.

The F_2TCNQ complex (**6**) clearly exhibits a metallic temperature dependence even in the compressed pellet form down to 15 K, below which the resistivity increases gradually (Fig. 2). A plot of $\ln\rho$ against $T^{-1/4}$ below 12 K gives an excellent straight line, as expected for the three-dimensional variable-range hopping system.[28]

The resistivity of other complexes showing the MI transition (see Table 1) is rather temperature independent down to T_{MI} as demonstrated in Fig. 2 for **1a**, **11** and **17**. Particularly it should be noted that the resistivity of the TCNQ complex (**11**) remains invariant down to *ca.* 120 K (σ_{RT} = 7.7 S cm^{-1}), where it then begins to increase more rapidly. Thus the metallic state of **11** is thermodynamically more stable relative to those of semiconductive (BO)(TCNQ)[7a] and triclinic (ET)(TCNQ) with a MI transition at 330 K.[24b] The ε_a value of **11** below 100 K is evaluated to 22 meV, which is much smaller than those of (BO)(TCNQ) and (ET)(TCNQ) (40–70 meV).

Fig. 3a shows uniform segregated columns composed of individual component molecules in **11** (for crystallographic data of **11** and other complexes, see Table 2).¶ The TCNQ molecules form a bond-over-ring overlap mode with an interplanar spacing of 3.34 Å. The overlap integral $t1$ (13.3×10^{-3}) is more than 100 times those of other directions, indicating the one-dimensional electronic structure of the TCNQ part. The EOET molecules stack in a head-to-head manner with an interplanar spacing of 3.66–3.67 Å as seen in Fig. 3b. Such a stacking manner as to give short CH···O hydrogen bonds (dashed lines in Fig. 3a, 3.55 and 3.56 Å *vs.* van der Waals (vdW) distance of CH···O 3.72 Å[29]) is necessary for EOET molecules to self-assemble along the face-to-face direction. It is thus evident that the self-aggregation of the EOET molecules is exerted by the hydrogen bonds along the stack like that of the BO molecules.[7] A slip from each other along the molecular short axis (Fig. 3b) also resembles closely the BO compounds.[7a]

Each segregated EOET column also slips from the neighboring column along the molecular long axis, and no pronounced short S···S atomic contact is observed along the side-by-side direction contrary to many BO and ET compounds. The side-by-side S···S distances are 3.67 Å for $S_{in}\cdots S_{in}$ and 3.72 and 3.81 Å for $S_{in}\cdots S_{out}$. These values are slightly larger than the corresponding vdW distance (3.60 Å) due to the lower symmetry of EOET molecule and the relative orientation of EOET columns. Fig. 4 schematically demonstrates the typical S···S atomic contacts along the side-by-side direction in (a) BO, (b) EOET and (c) ET compounds where the molecular shapes are exaggerated for easy understanding. Since the HOMO coefficient of inner chalcogen atoms of BO, ET or EOET is generally 3–4 times greater than that of the outer chalcogen ones, the transfer interactions generated by $S_{in}\cdots S_{in}$ contacts along the side-by-side direction are significantly important compared to those by $S_{in}\cdots X_{out}$ and $X_{out}\cdots X_{out}$ contacts.[6a] For the BO compounds, the size difference between oxygen and sulfur atoms enables the formation of robust side-by-side $S_{in}\cdots S_{in}$ contacts, giving rise to a few particular patterns of X···X contacts (Fig. 4a). On the other hand, the $S_{in}\cdots S_{in}$ contacts are not so attainable in the usual ET compounds due to the steric hindrance exerted by bulky six-membered rings (for κ-phase, see Fig. 4c). Hence no particular $S_{in}\cdots S_{out}$ patterns are favorable and so various kinds of S···S contact are produced depending on the donor packing patterns (α-, β-, θ-, κ-phases, and so forth).[6,30] For complex **11**, the S···S contacts are not as effective for obtaining the transverse transfer interactions relative to those in the BO and ET

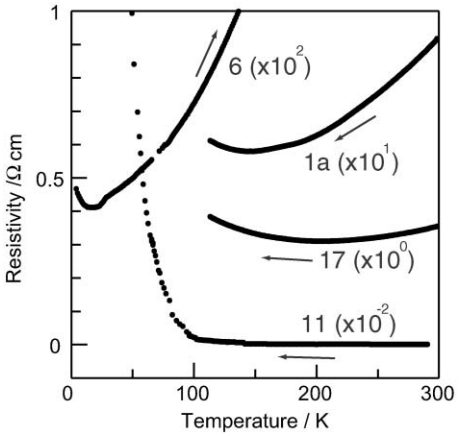

Fig. 2 Temperature dependence of resistivity on the compressed pellets for F_2TCNQ (**6**, the magnitude is multiplied by 10^2), HCBD (**1a**, $\times 10$) and *p*-QCl_4 (**17**, $\times 1$), and on single crystal for TCNQ (**11**, $\times 10^{-2}$) complexes among Group **A**.

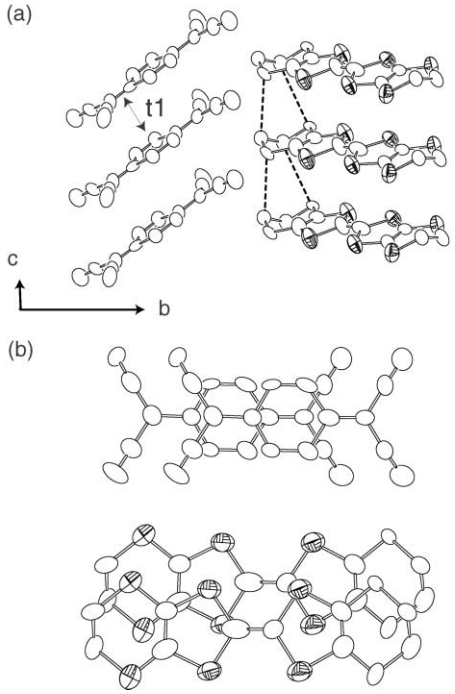

Fig. 3 (a) Crystal structure of (EOET)(TCNQ) (**11**) viewed along the *a**-axis. Short CH···O atomic contacts are shown by dashed lines. $t1$ is the calculated overlap integral between TCNQ molecules (13.3×10^{-3}) and is 100 times more than those of other directions. (b) Overlap modes of EOET and TCNQ molecules in each segregated column.

¶Crystal data for (EOET)(TCNQ), $(EOET)_2$(*p*-iodanil), $(EOET)_2$-$[(MeO)_2TCNQ]$, (EOET)(BTDA-TCNQ) and $(EOET)(BTDA\text{-}TCNQ)_2$ are available as supplementary data. CCDC reference numbers 175473–175477. See http://www.rsc.org/suppdata/jm/b1/b110605h/ for crystallographic files in .cif or other electronic format.

Table 2 Crystallographic data of EOET complexes with TCNQ (**11**), *p*-iodanil (**23**), $(MeO)_2$TCNQ (**16**) and BTDA-TCNQ (**20b**, **20c**)[a]

Complex	**11**	**16**	**20b**	**20c**	**23**
Acceptor (A)	TCNQ	$(MeO)_2$TCNQ	BTDA-TCNQ	BTDA-TCNQ	*p*-iodanil
EOET : A	1 : 1	2 : 1	1 : 1	1 : 2	2 : 1
Formula	$C_{22}H_{12}O_2N_4S_6$	$C_{34}H_{24}O_6N_4S_{12}$	$C_{22}H_8O_2N_8S_8$	$C_{34}H_8O_2N_{16}S_{10}$	$C_{26}H_{16}O_6S_{12}I_4$
Formula weight	556.76	969.38	672.89	993.20	1316.82
Crystal system	Triclinic	Triclinic	Monoclinic	Triclinic	Triclinic
Space group	$P1$	$P\bar{1}$	$P2_1/n$	$P1$	$P\bar{1}$
a/Å	7.213(3)	9.887(4)	7.620(1)	7.541(1)	8.120(1)
b/Å	19.856(5)	12.024(4)	12.973(2)	9.169(1)	12.000(1)
c/Å	4.041(1)	9.387(4)	13.247(2)	15.216(2)	10.967(1)
α/°	92.08(1)	94.75(3)		93.948(7)	69.558(4)
β/°	89.61(2)	109.87(4)	91.316(8)	101.680(6)	108.343(4)
γ/°	95.59(1)	103.17(7)		106.924(8)	104.786(4)
V/Å^3	575.6(3)	1006.2(7)	1309.2(3)	976.5(2)	937.7(1)
Z	1	1	2	1	1
d_c/g cm^{-3}	1.61	1.60	1.71	1.69	2.33
μ/mm^{-1}	0.625	0.674	0.732	0.595	3.625
Diffractometer[b]	a	b	a	a	a
$2\theta_{max}$/°	55	50	55	55	50
No. of intensity measured	1822	4565	2517	3410	3576
Criterion for obsd reflections	$F_0 \geqslant 3\sigma(F_0)$	$F_0 \geqslant 4\sigma(F_0)$	$F_0 \geqslant 4\sigma(F_0)$	$F_0 \geqslant 2\sigma(F_0)$	$F_0 \geqslant 2\sigma(F_0)$
No. of refined parameters	304	256	193	540	217
R	0.057	0.055	0.070	0.068	0.033

[a]Diffraction data were collected at room temperature. [b]a: Mac Science DIP-2020K, b: Mac Science MXC$^{\kappa}$.

compounds owing to both the low-symmetric molecular shape and the ordered molecular orientation (Fig. 4b), where the latter is necessary for EOET molecules to obtain the longitudinal transfer interactions effectively. This is indicative of the reduced self-assembling ability of the EOET molecules with respect to the BO ones, and thereby facilitates the occurrence of the MI transition as observed for many complexes among this group. More precise characterizations concerning the relation between crystal and electronic structures, physical properties and the mechanism of the MI transition will be described elsewhere.

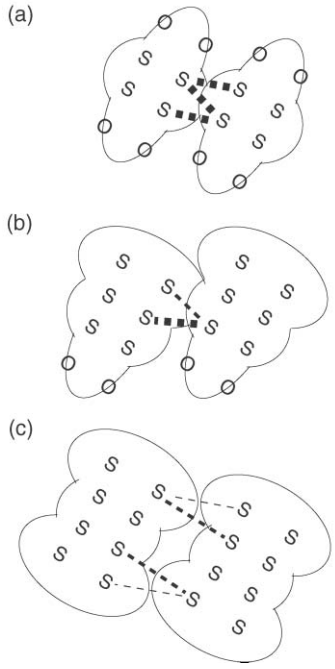

Fig. 4 Schematic figures of S···S atomic contacts in typical (a) BO, (b) EOET and (c) ET compounds. Dotted lines indicate the comparatively short S···S atomic contacts. Thick dotted lines: S_{in}···S_{in}, medium one: S_{in}···S_{out} and thin dotted lines: S_{out}···S_{out}. Examples are $(BO)_5(HCTMM)(PhCN)_2$,[7a] (EOET)(TCNQ) (**11**) and κ-$(ET)_2X$,[6] where HCTMM is hexacyanotrimethylenemethane. The S···S atomic contacts are less than the sum of the van der Waals radii for (a) BO and (c) ET compounds, but not for (b) EOET compound.

Group B. In the BO system, there is no compound with $h\nu_{CT}^{solid} > 5 \times 10^3$ cm^{-1} in the redox region of $-0.02 \leqslant \Delta E \leqslant 0.34$ V [eqn. (2)]. On the other hand, two EOET complexes along the V-shaped line were obtained in this redox region (**8**, **15**), and both exhibit an insulating character and thus are classified as a partial ionic CT complex with alternating stacks. This also indicates the reduced self-assembling ability of EOET molecules with respect to that of BO ones since the molecular self-aggregation would prefer segregated stacks rather than alternating ones. The insulating complexes **16**, **20b**, **20c**, **21** and **22** located in the range of eqn. (1) ($-0.25 \leqslant \Delta E \leqslant 0.60$ V) are also classified into Group **B**.

Fig. 5a shows the molecular structures in $(MeO)_2$TCNQ complex **16** viewed on the molecules. Both component molecules are almost flat and form DDA alternating columns (Fig. 5b). Since an inversion center is present at the center of the acceptor molecule, DAD is the repeating unit. The interplanar spacings of DD and DA along the stack are appropriate for a CT solid (3.56 Å and 3.50–3.54 Å, respectively). The head-to-tail stacking in a DD dimer results in the absence of the CH···O hydrogen bond, also there are no tight atomic contacts between EOET and $(MeO)_2$TCNQ molecules. The IR-active C≡N stretching mode that appeared at 2213 cm^{-1} is very close to that of neutral $(MeO)_2$TCNQ (2219 cm^{-1}) rather than that of anionic $(MeO)_2TCNQ^-$ (2198 and 2175 cm^{-1}), indicating a nearly neutral ionicity of **16**.

Single crystals of 1 : 1 (**20b**) and 1 : 2 (**20c**) BTDA-TCNQ complexes are obtained simultaneously by diffusion method and then separated under a microscope. However, attempts to obtain the single crystals of 3 : 2 complex (**20a**), which exhibits a high conductivity (23 S cm^{-1} at RT) and is classified into Group **A** (see Table 1), are presently unsuccessful.

Typical DA alternating stacks are established in the 1 : 1 BTDA-TCNQ complex (**20b**) (Fig. 6a). The orientation of EOET molecules is completely disordered and the donor plane is not parallel to the acceptor molecule but has a dihedral angle of 4.7°. The distance between two donor molecules along the stack is 6.95 Å.

As seen in Fig. 6b, a DA alternating column in the 1 : 2 BTDA-TCNQ complex (**20c**) is sandwiched by additional BTDA-TCNQ molecules. Similar to the 1 : 1 complex, the molecular planes of donor and acceptor in the same column are not parallel to each other but have a dihedral angle of 1.2°. The

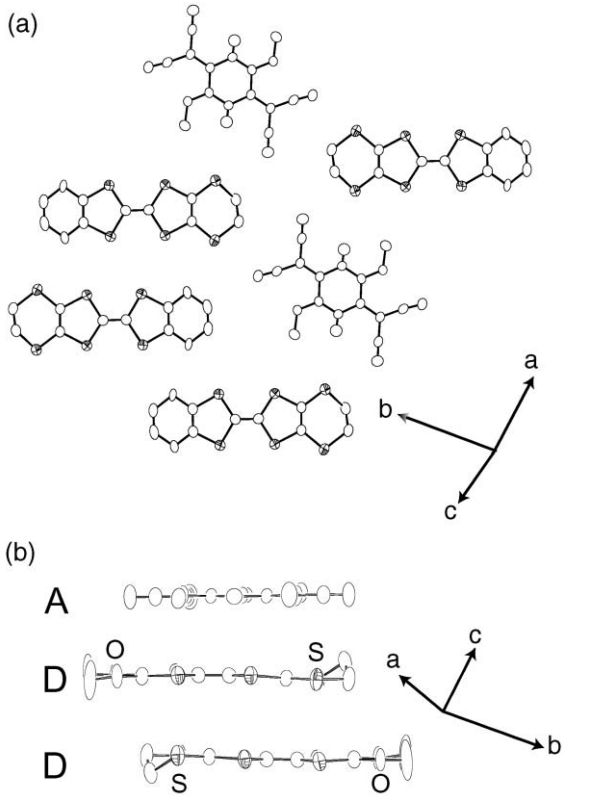

Fig. 5 Crystal structure of $(EOET)_2[(MeO)_2TCNQ]$ (**16**) (a) projected perpendicular to the molecular planes and (b) along the molecular short axes.

interplanar spacings of DD and DA along the stack are 6.89 Å and 3.38–3.42 Å, respectively.

Since the ν_{CN} mode at 2230 cm^{-1} in BTDA-$TCNQ^0$ redshifts to 2192 cm^{-1} in the anion radical salt Li^+(BTDA-$TCNQ^-$), BTDA-TCNQ molecules in the 3 : 2 complex (**20a**) with ν_{CN} = 2190–2192 cm^{-1} are in a completely ionized state. Also the charges on the BTDA-TCNQ molecules in the 1 : 1 (**20b**, ν_{CN} = 2220 cm^{-1}) and 1 : 2 (**20c**, ν_{CN} = 2226 cm^{-1}) complexes are evaluated to 0.3 and 0.1 respectively, on the assumption of a linear relation between the ν_{CN} mode and the charge on the BTDA-TCNQ molecules. Then the charges on EOET molecules are readily deduced to be *ca.* 0.7, 0.3 and 0.2 for the 3 : 2 (**20a**), 1 : 1 (**20b**) and 1 : 2 (**20c**) complexes, respectively.

Accordingly, the rather small degree of CT observed in **16**, **20b** and **20c** gives the alternating stacks and thereby the display of both the insulating character and the $h\nu_{CT}^{solid}$ values along the V-shaped line.

Group C. For complexes **18b**, **19**, **23**, **24b** and **26**, the $h\nu_{CT}^{solid}$ values substantially exceed the values expected from the V-shaped line by 2–4.5 × 10^3 cm^{-1}. The complexes **18b** and **19**, especially, are located far above the line by more than 4 × 10^3 cm^{-1}, which is evidently beyond the crystal field effect. Such a deviation is generally indicative of the different intermolecular interactions from the CT ones and/or the molecular packing depressing the Coulomb attractive energy.

The crystal structure of the *p*-iodanil (QI_4) complex (**23**) projected along the *b**-axis and along the molecular short axis of the EOET molecule are shown in Fig. 7a and 7b, respectively. Concave EOET and flat QI_4 molecules form a DDA alternating column along the (*a* + *c*) direction where a QI_4 molecule is encapsulated between two EOET molecules. Since both the center of the EOET dimer and the center of the QI_4 molecule are present at the inversion

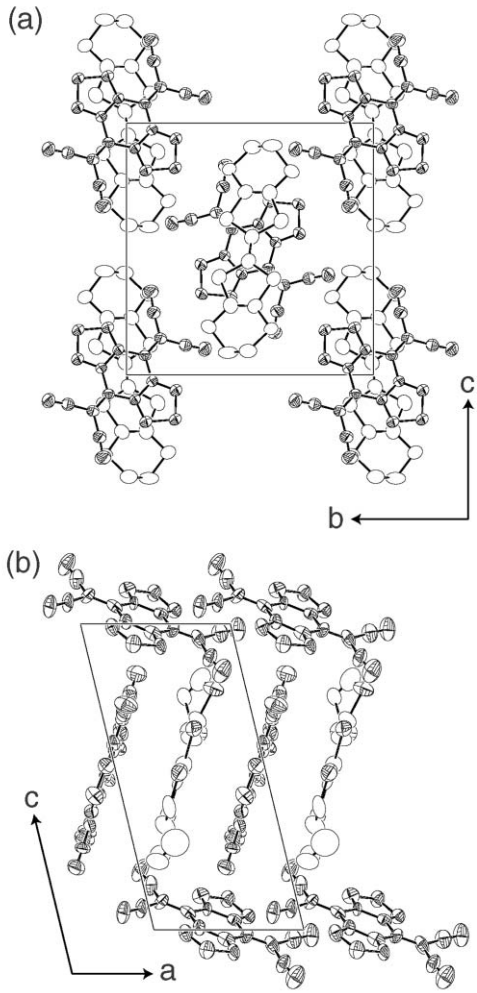

Fig. 6 Crystal structures of (a) 1 : 1 BTDA-TCNQ complex (**20b**) projected along the *a*-axis and (b) 1 : 2 complex (**20c**) projected along the *b*-axis.

center, the repeating unit of the complex is DAD in a fashion similar to that in the $(MeO)_2TCNQ$ complex (**16**). The molecular plane of QI_4 is not parallel to that of the central $C_6S_6O_2$ moiety in EOET with a dihedral angle of 13.4°. The EOET molecules form the head-to-tail stacking in the dimer, and so no hydrogen bond is available for the self-aggregation of EOET molecules in **23**.

The overlap patterns of DAD and those of DD in **23** viewed on the molecules are also depicted in Fig. 7c and 7d, respectively. The distance between the averaged EOET molecular planes is rather long (4.11 Å) although the overlap mode in the EOET dimer is distinctly close to a bond-over-ring type (Fig. 7d). For the overlap pattern of DAD (Fig. 7c), the distance between the center of the QI_4 molecule and the central tetrathioethylene in the EOET molecule is also significantly long (3.98 Å), and the quinone ring in the QI_4 molecule hardly overlaps with the EOET ones ($s1 = 0.41 \times 10^{-3}$, $s2 = 0.96 \times 10^{-3}$, see Fig. 7a). Naturally no short heteroatomic contact such as I···S (4.18–4.88 Å *vs.* vdW distance of 3.78 Å) or O···S (3.35–3.70 Å *vs.* vdW distance of 3.32 Å) is present between the EOET and QI_4 molecules. Thus complex **23** should be regarded as a clathrate-type compound rather than a conventional CT one. The IR-active $\nu_{C=O}$ mode that appeared at 1656 cm^{-1} resembles closely that in neutral QI_4 ($\nu_{C=O}$ = 1660 cm^{-1}), and the conductivity measurement indicates an insulating character ($\sigma_{RT} < 10^{-8}$ S cm^{-1}).

The observed large $h\nu_{CT}^{N}$ values in this group are readily interpreted as described previously, *i.e.*, the reduced Coulomb

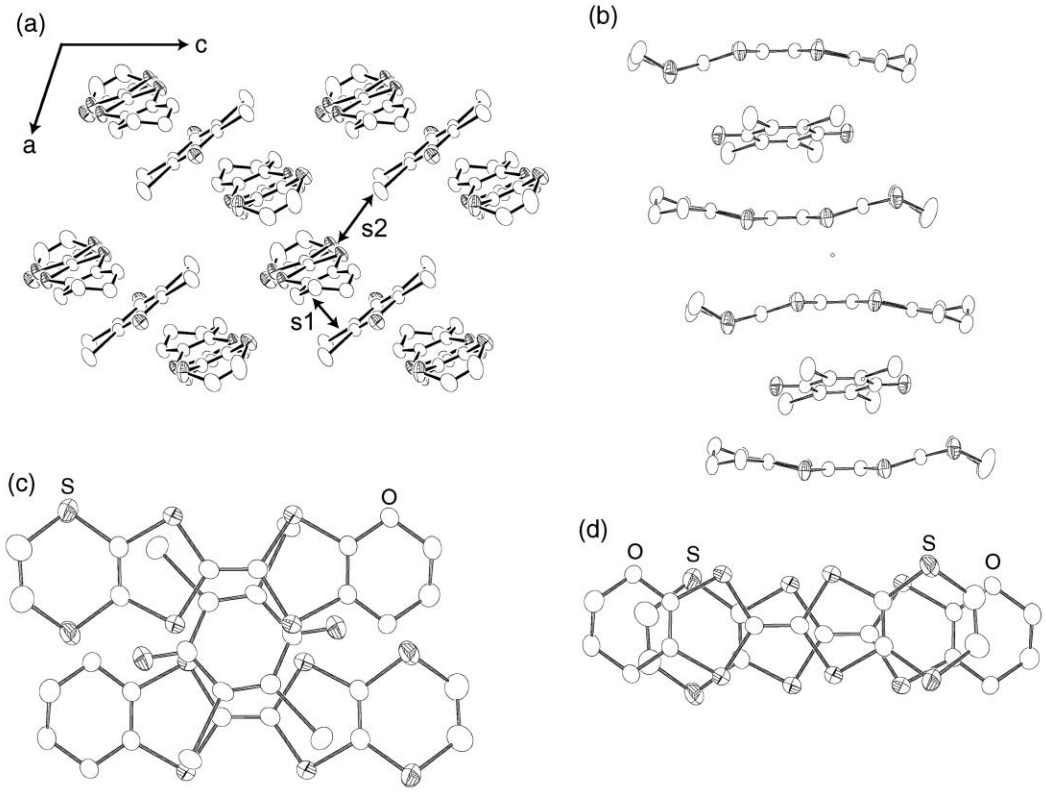

Fig. 7 Crystal structure of $(EOET)_2(QI_4)$ (**23**): (a) projected along the b*-axis; (b) along the molecular short axis of EOET molecule; (c) overlap mode of DAD; (d) overlap mode of DD. $s1$ and $s2$ are the overlap integrals between EOET and QI_4 molecules. Inversion centers are denoted as small open circles.

attractive interactions between component molecules (C) due to the molecular packing which is unfavorable for CT interactions according to eqn. (3),

$$h\nu_{CT}{}^{N} = I_P - E_A - C \quad (3)$$

where I_p and E_A are the ionization potential of the donor molecule and the electron affinity of the acceptor molecule, respectively. This situation is very reminiscent of the BO complex of H_2TNBP, in which intermolecular OH···O hydrogen bonds between H_2TNBP and BO molecules contribute mainly to the formation of the complex compared to the CT interactions, resulting in a distinct crystal structure among the BO compounds.[7a]

Based on their unexpectedly large $h\nu_{CT}{}^{solid}$ values together with the insulating characters and IR spectra exhibiting a superposition of individual component molecules (see Table 1), other complexes classified into this group (**18b**, **19**, **24b**, **26**) are also anticipated to have analogous structural features, although structural refinement is presently successful only for **23**.

Group D. Complexes **27**, **28a**, **28b**, **29** and **30** locate along the right side of the V-shaped line, indicating a neutral ground state with alternating stacks. Single crystals, enough to refine the crystal structures, are obtained only for the complexes with C_{60}, although the convergences are insufficient, likely due to the static or dynamic orientational disorder of C_{60} molecules (R values are 0.132 for **28a** and 0.208 for **28b**). Two structurally distinct 1 : 1 : 1(benzene) complexes, **28a** (block) and **28b** (plate), were identified by structural refinements. No distinguishing differences between both complexes are realized in IR, UV–Vis and conductivity measurements. The IR-active $F_{1u}(4)$ mode at 1428 cm^{-1} was unchanged on complex formation.

The crystal structures of **28a** and **28b** are analyzed with a restriction of the rigid model for all C_{60} molecules. Moreover, four and two disordered orientations are presumed for C_{60} molecules in **28a** and **28b** respectively, and the orientation of EOET molecules is completely disordered in both complexes. For complex **28a**, the crystallographic data are: monoclinic, space group $C2/c$, $a = 16.512(3)$, $b = 13.577(1)$, $c = 20.843(3)$ Å, $\beta = 102.193(6)^\circ$, $V = 4567(1)$ Å^3, $Z = 4$, $R = 0.138$. Fig. 8a shows the molecular packing projected on to the bc-plane. The C_{60} molecules form one-dimensional columns along the

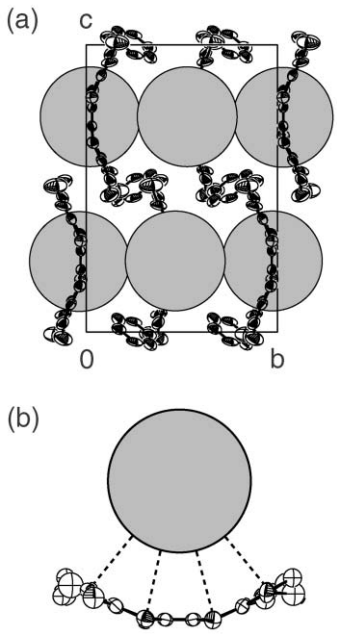

Fig. 8 (a) Crystal structure of the monoclinic phase of $(EOET)(C_{60})$-(benzene) (**28a**) projected along the a-axis. (b) van der Waals atomic contacts between EOET and C_{60} molecules (dashed lines) where the C_{60} molecule is represented as a circle.

c-axis with the distance between the centers of the fullerene sphere equal to 10.42 Å. Each C_{60} molecule forms a DA pair with a concave EOET molecule and the shortest intermolecular C···S or C···O atomic contacts (3.49–3.59 Å) are comparable to the vdW distance of C···S (3.55 Å) as shown by dotted lines in Fig. 8b. For EOET molecules, the dihedral angle between the central C_2S_4 moiety and adjacent $C_2S_2X_2$ (X = O or S) moiety is 22.7°. Neighboring DA columns along the *b*-axis are arranged with oppositely oriented EOET molecules. The crystal structure is essentially analogous to that of (DBTTF)(C_{60})(benzene).[31]

For complex **28b**, the crystallographic data are: triclinic, space group $P\bar{1}$, $a = 10.155(1)$, $b = 10.289(1)$, $c = 11.189(2)$ Å, $\alpha = 78.390(7)$, $\beta = 78.102(5)$, $\gamma = 84.129(7)°$, $V = 1118.3(2)$ Å^3, $Z = 1$, $R = 0.226$. As shown in Fig. 9, the C_{60} molecules form a two-dimensional network in the *ab*-plane with the distances between the centers of the fullerene sphere equal to 10.16 Å ($\|a$) and 10.29 Å ($\|b$). The formation of the C_{60} two-dimensional layer[32] is particularly fascinating for molecular solids, since such a segregated layer would be unfavorable for the neutral CT complex composed of conventional molecules bearing no hetero atoms.[22b,33] The vacancies between the C_{60} layers contain planar EOET and benzene molecules, whose centers are present at (1/2,0,0) and (0,1/2,0), respectively. Along the [011] and [01$\bar{1}$] directions, the EOET and C_{60} molecules are arranged as DA alternating stacks, in which the shortest intermolecular C···S or C···O atomic contacts (3.13–3.71 Å) are comparable to the vdW distances of C···S (3.55 Å) and C···O (3.20 Å). These alternating stacks give rise to the CT absorption band expected from the V-shaped line. The molecular packing is essentially similar to that of (OMTTF)(C_{60})(benzene).[32c]

Group E. Insulating complexes **1b** and **2** with 1 : 1 stoichiometry locate in the vicinity of the left side of the V-shaped line, as expected for a fully ionic ground state with alternating stacks. However, the UV–Vis–NIR spectrum of F_4TCNQ complex (**2**) in KBr pellet exhibits two distinct absorption bands characteristic of intermolecular transitions between each $EOET^+$ and F_4TCNQ^- radicals (9.0×10^3 cm^{-1} for $EOET^+$ and 6.7×10^3 cm^{-1} for F_4TCNQ^-), indicating the formation of segregated columns composed of individual fully ionized component molecules. The intermolecular transition energy between $EOET^+$ radicals is intermediate between those of BO^+ (7–10 $\times 10^3$ cm^{-1} for $(BO)_2Br(H_2O)_3$) and ET^+ (6×10^3 cm^{-1} for $(ET)Br(H_2O)$).[20]

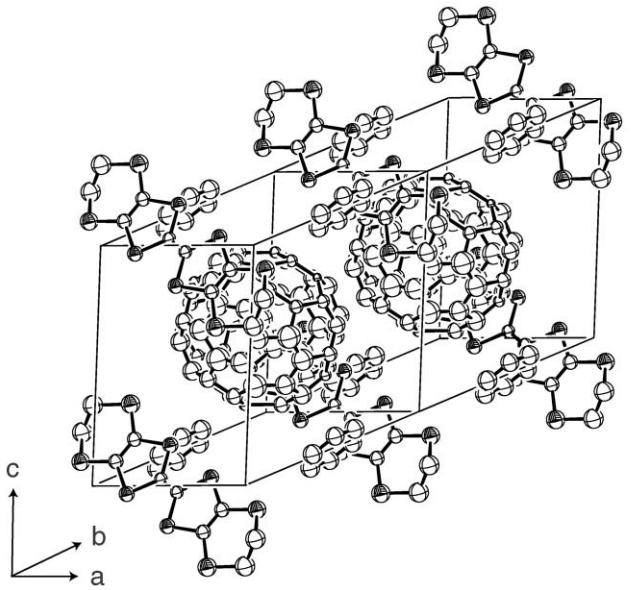

Fig. 9 Crystal structure of triclinic phase of (EOET)(C_{60})(benzene) (**28b**).

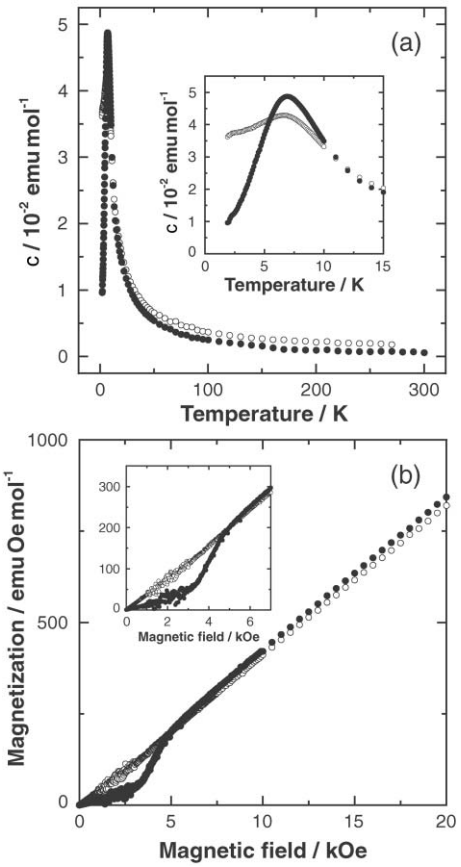

Fig. 10 (a) Temperature dependence of static susceptibility of polycrystalline (EOET)(F_4TCNQ) (**2**) in an applied magnetic field of 1 kOe. The magnetic fields are applied along the directions approximately parallel ($H_\|$, ●) and perpendicular ($H_\perp$, ○) to the needle axes of crystals. Inset is the enlargement for the low temperature range. (b) Magnetic field dependence of magnetization at 1.9 K. Inset is the enlargement for the low magnetic field range.

The anisotropy of static susceptibility χ in **2** (polycrystalline needles) as a function of temperature is demonstrated in Fig. 10a. The magnetic field (0.1 T) was applied along the directions approximately parallel ($\|$) and perpendicular ($\perp$) to the needle axes of the crystals. Both $\chi_\|$ and $\chi_\perp$ follow the Curie-like law above *ca.* 10 K, and take a maximum at around 7 K. Below the temperature, $\chi_\|$ decreases rapidly toward zero, while a more gradual decrease of susceptibility was observed in $\chi_\perp$. The anisotropic susceptibility below the transition temperature immediately rules out the occurrence of a finite spin-gap such as a spin–Peierls transition, which has been previously reported for the F_4TCNQ complexes of HMTXF (X = S, Se).[34] As seen in Fig. 10b, a spin–flop transition characteristic of an antiferromagnetic spin structure is observed at *ca.* 3 kOe, which is comparable to *ca.* 5 kOe in $(TMTSF)_2MF_6$ (M = P, As) with a spin density wave (SDW) ground state[35] and *ca.* 3 kOe in κ-$(ET)_2Cu[N(CN)_2]Cl$ with a canted antiferromagnetic ground state.[36] Considering that both F_4TCNQ complexes of BO and ET exhibit an antiferromagnetic ordering below the Néel temperature (T_N)[37] and that the transition temperature in **2** (7 K) is intermediate between those of (BO)(F_4TCNQ) (5.4 K)[37a] and (ET)-(F_4TCNQ) (14 K),[37b] the magnetic ground state in **2** below 7 K is readily attributed to the antiferromagnetism. Then it appears that the easy axis is approximately along the needle axis of the crystal. The possible high electronic dimensionality of **2** with respect to those of (HMTXF)(F_4TCNQ) (X = S, Se)

may be responsible for the occurrence of the antiferromagnetic ordering rather than the spin–Peierls one.

3 Conclusion and summary

By using an EOET molecule which is a hybrid between BO and ET, 36 kinds of CT complex were prepared with conventional organic acceptor molecules and classified into five groups (**A**–**E**). Owing to the existence of the self-aggregation of EOET molecules, 17 kinds of highly conductive complex (Group **A**) are scattered in the extensive redox range ($-0.25 \leqslant \Delta E \leqslant 0.60$ V) in a fashion similar to the corresponding BO ones. However, the formation of the complexes classified into Groups **B** (partially ionic insulator with alternating stacks, 7 complexes) and **C** (neutral clathrate with high $h\nu_{CT}^{solid}$, 5 complexes), both of which are rarely found in BO compounds, is strongly indicative of the reduced self-assembling ability of EOET molecules compared to BO ones. This reduction is adequate to rationalize the appearance of polymorphism and the MI transition, both of which have been realized largely for ET compounds rather than BO ones. On the other hand, Groups **D** and **E** contain five completely neutral and two completely ionic CT complexes, respectively. In conclusion, the EOET molecules substantially inherit the typical characteristics of the corresponding BO and ET and allow for a structurally and electronically wide variety of molecular complexes.

4 Experimental

Materials

All the donor and acceptor molecules including commercially available ones were purified by recrystallization and/or sublimation. Solid CT complexes were prepared either by direct mixing or by diffusion methods in appropriate solvents (CH_3CN, tetrahydrofuran or benzene).

Measurements

Optical measurements were carried out on KBr disks on a Perkin-Elmer 1000 Series FT-IR (resolution 4 cm^{-1}) for IR and near-IR regions (400–7800 cm^{-1}) and on a Shimadzu UV-3100 spectrometer for near-infrared, visible and ultraviolet (UV–Vis–NIR) regions (3800–42000 cm^{-1}). For single crystals, the temperature dependence of IR spectra was measured with the aid of a Nicolet 800 FT-IR (800–7800 cm^{-1}, 9–300 K).

CV measurements were performed in CH_3CN solution with 0.1 M (TBA)(BF_4) with a Yanaco Polarographic Analyzer P-1100. The working and counter electrodes were Pt, the reference electrode was SCE, and the scan rate was 20 mV s^{-1}.

DC conductivities were measured by a standard four- or two-probe technique by attaching gold wires (10 μm diameter) to the samples with gold paint (Tokuriki Kagaku, 8560-1A).

A Quantum Design MPMS–XL SQUID magnetometer was used to collect the magnetization data down to 1.9 K.

X-Ray diffraction data were collected on imaging plate type or automatic four circle diffractometers (Mac Science DIP-2020K, Mac Science MXC$^{\kappa}$) with graphite monochromated Mo Kα radiation at RT. Crystal structures were solved by direct methods (SIR92) and refined by full matrix least-squares method on F or F^2 (SHELXL-93).[38] The position of the hydrogen atoms of EOET was determined assuming sp^3 configuration with a C–H distance of 1.0 Å. The refined and calculated atomic parameters are summarized as supplementary materials.¶

Acknowledgement

This work was in part supported by a Grant-in-Aid for Scientific Research from the Ministry of Education, Science, Sports, and Culture, Japan (12CE2005), a Grant for CREST (Core Research for Evolutional Science and Technology) of Japan Science and Technology Corporation (JST), a fund for "Research for the Future" from the Japan Society for Promotion of Science and a fund for the International Joint Research Grant Program of the New Energy and Industrial Technology Development Organization (NEDO).

References

1 Proceedings of International Conferences on Science and Technology of Synthetic Metals (ICSM): (*a*) *J. Phys.*, 1983, **44**, C3, Les Arcs, 1982; (*b*) *Mol. Cryst. Liq. Cryst.*, 1985, **117–121**, Abano Terme, 1984; (*c*) *Synth. Met.*, 1987, **17–19**, Kyoto, 1986; (*d*) *Synth. Met.*, 1991, **41–43**, Tübingen, 1990; (*e*) *Synth. Met.*, 1993, **55–57**, Göteborg, 1992; (*f*) *Synth. Met.*, 1995, **69–71**, Seoul, 1994; (*g*) *Synth. Met.*, 2001, **120**, Bad Gastein, 2000.

2 (*a*) K. Kanoda, K. Akiba, T. Takahashi, K. Suzuki and G. Saito, *Phys. Rev. Lett.*, 1990, **65**, 1271; (*b*) L. P. Lee, G. M. Luke, B. J. Sternlief, W. D. Wu, Y. J. Uemura, J. H. Brewer, T. M. Riseman, C. E. Stronach, G. Saito, H. Yamochi, H. H. Wang, A. M. Kini, K. D. Carlson and J. M. Williams, *Phys. Rev. Lett.*, 1992, **68**, 1923; (*c*) K. Ichimura, T. Arai, K. Nomura, S. Takahashi, J. Yamada, S. Nakatsuji and H. Anzai, *Physica C*, 1997, **282–287**, 1895; (*d*) J. M. Schrama, E. Rzepniewski, R. Edwards, J. Singleton, A. Ardavan, M. Kurmoo and P. Day, *Phys. Rev. Lett.*, 1999, **83**, 3041. However, the symmetry of the superconducting state is still controversial: (*e*) H. Elsinger, J. Wosnitza, S. Wanka, J. Hagel, D. Schweitzer and W. Strunz, *Phys. Rev. Lett.*, 2000, **84**, 6098.

3 (*a*) M. V. Kartsovnik, P. A. Kononovich, V. N. Laukhin and I. F. Schegolev, *Pis'ma Zhur. Eks. Teor. Fiz.*, 1988, **48**, 498; (*b*) K. Kajita, Y. Nishio, T. Takahashi, R. Kato, H. Kobayashi, W. Sasaki, A. Kobayashi and Y. Iye, *Solid State Commun.*, 1989, **70**, 1189; (*c*) K. Yamaji, *J. Phys. Soc. Jpn.*, 1989, **58**, 1520.

4 (*a*) T. Nakamura, G. Yunome, R. Azumi, M. Tanaka, H. Tachibana, M. Matsumoto, S. Horiuchi, H. Yamochi and G. Saito, *J. Chem. Phys.*, 1994, **98**, 1882; (*b*) K. Ogasawara, T. Ishiguro, S. Horiuchi, H. Yamochi and G. Saito, *Jpn. J. Appl. Phys.*, 1996, **35**, L571; (*c*) H. Ohnuki, T. Noda, M. Izumi, T. Imakubo and R. Kato, *Phys. Rev. B*, 1997, **55**, R10225.

5 (*a*) A. Tracz, J. K. Jeszka, A. Sroczynska, J. Ulanski, J. Plocharski, H. Yamochi, S. Horiuchi and G. Saito, *Synth. Met.*, 1997, **86**, 2173; (*b*) S. Horiuchi, H. Yamochi, G. Saito, J. K. Jeszka, A. Tracz, A. Sroczynska and J. Ulanski, *Mol. Cryst. Liq. Cryst.*, 1997, **296**, 365; (*c*) J. K. Jeszka, A. Tracz, A. Sroczynska, M. Kryszewski, H. Yamochi, S. Horiuchi, G. Saito and J. Ulanski, *Synth. Met.*, 1999, **106**, 75.

6 (*a*) T. Ishiguro, K. Yamaji and G. Saito, *Organic Superconductors*, 2nd edn., Springer, Berlin, 1998; (*b*) J. M. Williams, J. R. Ferraro, R. J. Thorn, K. D. Carlson, U. Geiser, H. H. Wang, A. M. Kini and M.-H. Whangbo, *Organic Superconductors including Fullerenes*, Prentice Hall, Englewood Cliffs, 1992.

7 (*a*) S. Horiuchi, H. Yamochi, G. Saito, K. Sakaguchi and M. Kusunoki, *J. Am. Chem. Soc.*, 1996, **118**, 8604; (*b*) F. Wudl, H. Yamochi, T. Suzuki, H. Isotalo, C. Fite, H. Kasmai, K. Liou, G. Srdanov, P. Coppens, K. Maly and A. Frost-Jensen, *J. Am. Chem. Soc.*, 1990, **112**, 2461; (*c*) M. A. Beno, H. H. Wang, A. M. Kini, K. D. Carlson, U. Geiser, W. K. Kwok, J. E. Thompson, J. M. Williams, J. Ren and M.–H. Whangbo, *Inorg. Chem.*, 1990, **29**, 1599; (*d*) S. Kalich, D. Schweitzer, I. Heinen, E. L. Song, B. Nuber, H. J. Keller, K. Winzer and H. W. Helberg, *Solid State Commun.*, 1991, **80**, 191; (*e*) M.–H. Whangbo, D. Jung, J. Ren, M. Evain, J. J. Novoa, F. Mota, S. Alvarez, J. M. Williams, M. A. Beno, A. M. Kini, H. H. Wang and J. R. Ferraro, *The Physics and Chemistry of Organic Superconductors*, eds. G. Saito and S. Kagoshima, p. 262, Springer-Verlag, Berlin, 1990.

8 H. Mori, S. Tanaka and T. Mori, *Phys. Rev. B*, 1998, **57**, 12023.

9 H. Sasaki, T. Kondo, K. Kamoshida, Y. Sacho and G. Saito, *Synth. Met.*, 1999, **102**, 1626.

10 A. M. Kini, T. Mori, U. Geiser, S. M. Budz and J. M. Williams, *J. Chem. Soc., Chem. Commun.*, 1990, 647.

11 A. Otsuka, G. Saito, S. Hirate, S. Pac, T. Ishida, A. A. Zakhidov and K. Yakushi, *Mater. Res. Soc. Symp. Proc.*, 1998, **488**, 495.

12 A. Terzis, A. Hountas, B. Hilti, C. Mayer, J. S. Zambounis, D. Lagouvardos, V. C. Kakoussis, G. Mousdis and G. C. Papavassiliou, *Synth. Met.*, 1995, **41–43**, 1715.
13 S. V. Konovalikhin, G. V. Shilov, E. I. Zhilyaeva, S. A. Torunova and R. N. Lyubovskaya, *Russ. J. Coord. Chem.*, 2000, **26**, 89.
14 H. Ohnuki, T. Noda, M. Izumi, T. Imakubo and R. Kato, *Supramol. Sci.*, 1997, **4**, 413.
15 G. C. Papavassiliou, D. Lagouvardos, V. C. Kakoussis, A. Terzis, A. Hountas, B. Hilti, C. Mayer, J. S. Zambounis, J. Pffeiffer, M.–H. Whangbo, J. Ren and D. B. Kang, *Mater. Res. Soc. Symp. Proc.*, 1992, **247**, 535.
16 L. Ducasse, G. Mousdis, M. Fettouhi, L. Ouahab, J. Amiell and P. Delhaes, *Synth. Met.*, 1993, **55–57**, 1995.
17 G. C. Papavassiliou, V. C. Kakoussis, D. J. Lagouvardos and G. A. Mousdis, *Mol. Cryst. Liq. Cryst.*, 1990, **181**, 171.
18 T. Mori, H. Inokuchi, A. M. Kini and J. M. Williams, *Chem. Lett.*, **1990**, 1279.
19 J. B. Torrance, J. E. Vazquez, J. J. Mayerle and V. Y. Lee, *Phys. Rev. Lett.*, 1981, **46**, 253.
20 T. Senga, K. Kamoshida, L. A. Kushch, G. Saito, T. Inamoto and I. Ono, *Mol. Cryst. Liq. Cryst.*, 1997, **296**, 97.
21 K. Nakasuji, *Pure Appl. Chem.*, 1990, **62**, 477.
22 (*a*) H. M. McConnell, B. A. Hoffman and R. M. Metzger, *Proc. Natl. Acad. Sci. USA*, 1965, **53**, 46; (*b*) F. H. Herbstein, *Perspectives in Structural Chemistry*, eds. J. D. Dunitz and J. A. Ibers, Vol. 4, p. 166, Wiley, New York, 1971.
23 G. Saito and J. P. Ferraris, *Bull. Chem. Soc. Jpn.*, 1980, **53**, 2141.
24 (*a*) G. Saito, H. Hayashi, T. Enoki and H. Inokuchi, *Mol. Cryst. Liq. Cryst.*, 1985, **120**, 341; (*b*) T. Mori and H. Inokuchi, *Solid State Commun.*, 1986, **59**, 355; (*c*) T. Mori and H. Inokuchi, *Bull. Chem. Soc. Jpn.*, 1987, **60**, 402; (*d*) Y. Iwasa, K. Mizuhashi, T. Koda, Y. Tokura and G. Saito, *Phys. Rev. B*, 1994, **49**, 3580.
25 J. R. Andersen, R. A. Craven, J. E. Weidenbronner and E. M. Engler, *J. Chem. Soc., Chem. Commun.*, 1977, 526.
26 (*a*) K. Bechgaard, D. O. Cowan and A. N. Bloch, *J. Chem. Soc., Chem. Commun.*, 1974, 937; (*b*) T. J. Kistenmacher, T. J. Emge, A. N. Bloch and D. O. Cowan, *Acta Crystallogr., Sect. B*, 1982, **38**, 1193.
27 O. Drozdova, H. Yamochi, K. Yakushi, M. Uruichi, S. Horiuchi and G. Saito, *J. Am. Chem. Soc.*, 2000, **122**, 4436.
28 L. F. Mott, *Metal–Insulator Transitions*, Taylor & Francis Ltd., London, 1974.
29 A. Bondi, *J. Phys. Chem.*, 1964, **86**, 441.
30 H. Yamochi, T. Komatsu, N. Matsukawa, G. Saito, T. Mori, M. Kusunoki and K. Sakaguchi, *J. Am. Chem. Soc.*, 1993, **115**, 11319.
31 D. V. Konarev, Y. V. Zubavichus, Yu. L. Slovokhotov, Yu. M. Shul'ga, V. N. Semkin, N. V. Drichko and R. N. Lyubovskaya, *Synth. Met.*, 1998, **92**, 1.
32 (*a*) Q. Zhu, D. E. Cox, J. E. Fischer, K. Kniaz, A. R. McGhie and O. Zhou, *Nature*, 1992, **355**, 712; (*b*) J. D. Crane, P. B. Hitchcock, H. W. Kroto, R. Taylor and D. R. M. Walton, *J. Chem. Soc., Chem. Commun.*, 1992, 1764; (*c*) G. Saito, T. Teramoto, A. Otsuka, Y. Sugita, T. Ban, M. Kusunoki and K. Sakaguchi, *Synth. Met.*, 1994, **64**, 359; (*d*) R. E. Douthwaite, M. L. H. Green, S. J. Heyes, M. J. Rosseinsky and J. F. Turner, *J. Chem. Soc., Chem. Commun.*, 1994, 1367; (*e*) J. Llacay, J. Tarres, C. Rovira, J. Veciana, M. Mas and E. Molins, *J. Phys. Chem. Solids*, 1997, **58**, 1675.
33 (*a*) R. Foster, *Organic Charge-Transfer Complexes*, Academic Press, London, 1969; (*b*) D. O. Cowan, *New Aspects of Organic Chemistry – I. Proceedings of the 4th International Kyoto Conference on New Aspects of Organic Chemistry*, eds. Z. Yoshida, T. Shiba and Y. Ohshiro, Kodansha, Tokyo, 1989.
34 (*a*) J. B. Torrance, J. J. Mayerle, K. Bechgaard, B. B. Silverman and Y. Tomkiewicz, *Phys. Rev. B*, 1980, **22**, 4960; (*b*) M. E. Hawley, T. O. Poehler, T. F. Carruther, A. N. Bloch, D. O. Cowan and T. J. Kistenmacher, *Bull. Am. Phys. Soc.*, 1978, **23**, 424; (*c*) J. B. Torrance, Y. Tomkiewicz, R. Bozio, C. Pecile, C. R. Wolfe and K. Bechgaard, *Phys. Rev. B*, 1982, **26**, 2267.
35 (*a*) K. Mortensen, Y. Tomkiewicz, T. D. Schultz and E. M. Engler, *Phys. Rev. Lett.*, 1981, **46**, 1234; (*b*) K. Mortensen, Y. Tomkiewicz and K. Bechgaard, *Phys. Rev. B*, 1982, **25**, 3319.
36 K. Miyagawa, A. Kawamoto, Y. Nakazawa and K. Kanoda, *Phys. Rev. Lett.*, 1995, **75**, 1174.
37 (*a*) S. Horiuchi, Thesis, Kyoto University, 1997; (*b*) T. Hasegawa, K. Inukai, S. Kagoshima, T. Sugawara, T. Mochida, S. Sugiura and Y. Iwasa, *Synth. Met.*, 1997, **86**, 1801.
38 (*a*) A. Altomare, G. Cascarano, C. Giacovazzo, A. Guagliardi, M. C. Burla, G. Polidori and M. Camalli, SIR92, adapted by S. Mackay for Crystan-GM, MAC Science Co. Ltd., 1995; (*b*) G. M. Sheldrick, SHELXL-93, University of Göttingen, 1993.